Int. J. Heat Mass Transfer. Vol. 29, No. 6, pp. 819–830, 1986
Printed in Great Britain

0017–9310/86 $3.00 + 0.00
Pergamon Journals Ltd.

Natural convection in a vertical channel vented to the ambient through an aperture in the channel wall

L. F. A. AZEVEDO and E. M. SPARROW
Department of Mechanical Engineering, University of Minnesota, Minneapolis, MN 55455, U.S.A.

(*Received* 10 *September* 1985 *and in final form* 21 *November* 1985)

Abstract—Natural convection in a one-sided-heated, vertical channel in the presence of a vent opening in the unheated wall was studied both experimentally and numerically. The experiments were performed in water ($Pr \cong 5$) for parametric variations of the interwall spacing, vent opening size, vent axial position, and wall-to-ambient temperature difference (Rayleigh number). For comparison purposes, baseline data were also obtained for unvented channels. The heat transfer data were supplemented by cross-channel temperature distribution measurements and by flow visualization performed using the thymol blue electrochemical technique. The numerical solutions provided information on both the local and average Nusselt numbers, cross-channel temperature profiles, and the rates of fluid flow through the opening at the bottom of the channel and through the vent. Both the experiments and the numerical solutions demonstrated that the average Nusselt numbers for the channel are insensitive to both the vent opening size and the vent axial position, for the range of operating conditions investigated. The numerical solutions showed that although the mass flow rate entering the channel through the opening at the bottom decreases in response to the presence of the vent, the total mass flow rate drawn into the channel is very little affected. The local Nusselt number distributions exhibited sharp, vent-related peaks. Excellent agreement prevailed between the experimentally and numerically determined cross-channel temperature profiles. For certain operating conditions, the flow visualization experiments revealed the existence of a recirculation zone inside the channel, adjacent to the lower edge of the vent opening.

INTRODUCTION

NATURAL convection in one-sided-heated, vertical channels is encountered in many practical applications and has been the subject of numerical and experimental studies (e.g. [1–3]). These works, however, are restricted to channels which are open to the ambient only at the top and bottom. Of comparable practical relevance is the one-sided-heated channel which is vented by the presence of additional openings in the walls. These vents provide alternative paths for the ambient fluid to be drawn into the channel. Despite its wide applicability, especially in the cooling of electronic equipment, a literature survey revealed no prior work related to natural convection in vented channels.

The present paper is a combined experimental and numerical study of the heat transfer characteristics of one-sided-heated, vented channels. The investigated channel geometry consisted of an isothermal heated wall and an unheated wall in which a single slit-like vent was present. In this configuration, fluid from the ambient can be drawn into the channel through both the principal opening (at the bottom of the channel) and through the vent opening. To assess the heat transfer and fluid flow ramifications of the presence of the vent, parameteric variations were made of the interwall spacing, vent opening size, and vent axial position. For each configuration defined by these geometric parameters, the wall-to-ambient temperature difference (i.e. the Rayleigh number) was varied by an order of magnitude. For comparison purposes, baseline results were also obtained for unvented channels.

The heat transfer experiments encompassed the determination of average Nusselt numbers for the heated wall and the measurement of cross-channel temperature profiles at different axial positions within the channel. The experiments were conducted in water ($Pr \cong 5$). The numerical solutions provided both local and average Nusselt numbers, cross-channel temperature distributions, and the flow rates of the fluid entering the channel through the principal opening and the vent opening.

Flow visualization experiments were performed utilizing an electrochemically generated tracer fluid (thymol blue method) and were intended to reveal the patterns of fluid flow in the vicinity of the vent opening. For certain operating conditions, zones of recirculating flow inside the channel were observed and documented.

EXPERIMENTAL APPARATUS AND PROCEDURE

The test section

The description of the test section utilized in the experiments is facilitated by the schematic view presented in Fig. 1. The ventilated channel under study was bounded by two principal walls. One of these, the heated wall, designed to deliver heat isothermally to the fluid, was a 0.635-cm-thick copper plate with

NOMENCLATURE

A	surface area of the heated wall
g	acceleration of gravity
Gr_s	Grashof number, $g\beta(T_w - T_\infty)S^3/\nu^2$
H	channel height, Fig. 1
h	average heat transfer coefficient, equation (1)
k	thermal conductivity of water
$\dot{m}_{no/vent}$	mass flow rate passing through the unvented channel
$\dot{m}_o$	mass flow rate passing through the principal opening of the vented channel
$\dot{m}_{tot}$	total mass flow rate drawn into the vented channel
Nu_{loc}	local Nusselt number, equation (20)
Nu_s	average Nusselt number, hS/k
P	dimensionless pressure difference, equation (8)
Pr	Prandtl number
p	pressure in channel
p_∞	pressure in ambient
p'	pressure difference, $(p - p_\infty)$
Q	rate of heat transfer at the heated wall
q	local rate of heat transfer per unit area at the heated wall
Ra_s	Rayleigh number, Gr_sPr
S	interwall spacing, Fig. 1
T	temperature
T_w	temperature of heated wall
T_∞	ambient temperature
t	vent opening size, Fig. 1
U, V	dimensionless velocity components, equation (7)
U_o	dimensionless inlet velocity
u, v	velocity components
u_o	inlet velocity
X, Y	dimensionless coordinates, equation (6)
X_v	dimensionless vent axial position
x, y	coordinates, Fig. 3
x_v	vent axial position, Fig. 3.

Greek symbols

β	coefficient of thermal expansion
θ	dimensionless temperature, equation (8)
ν	kinematic viscosity
ρ	fluid density in the channel
ρ_∞	fluid density in the ambient.

dimensions 14.54 × 9.67 cm (height × width). Heating of the plate was accomplished by means of three independently controlled heaters. Each heater consisted of Teflon-coated chromel wire (0.0127-cm diameter) laid in horizontal grooves machined on the back surface of the copper plate.

Each heater extended over a specific portion of the plate height. The first heater encompassed the lowermost four grooves, the second heater the middle seven grooves, and the third heater the top 10 grooves. This heating layout was designed to respond to the expected non-uniform heating required to attain a uniform wall temperature.

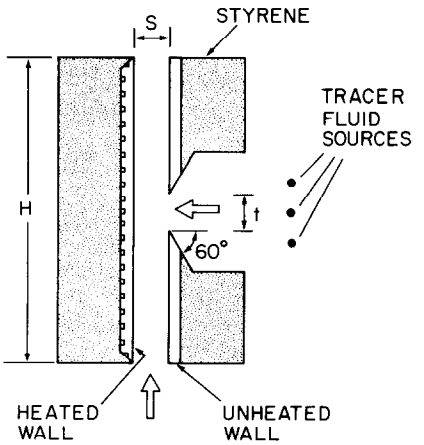

FIG. 1. Schematic side view of the experimental apparatus.

Temperature uniformity at the heating surface was obtained by carefully adjusting the power delivered to each heating circuit. Eight pre-calibrated chromel–constantan thermocouples (0.0254-cm diam.) were installed in the plate to guide the adjustment process. The thermocouples were installed in holes drilled into the rear face of the copper plate with their junctions situated 0.05 cm from the front face of the plate. A digital voltmeter with an accuracy of 1 μV was utilized in the voltage readings.

In all the runs performed, local deviations from the mean plate temperature were less than 1.5% of the wall-to-ambient temperature difference, with the typical deviation being 0.75%.

In order to minimize extraneous heat losses, the copper plate was backed by a 3.2-cm-thick, closed-pore, water-tolerant styrene block. As can be seen in Fig. 1, the upper and lower edges of the copper plate were beveled and covered with styrene insulation so that only the front surface of the plate contacted the water.

The unheated wall consisted of separate upper and lower portions as seen in Fig. 1. The space between the two parts of the wall formed the vent through which fluid was drawn into the vertical channel. Each portion of the unheated wall was constructed of a 0.635-cm-thick, 9.67-cm-wide Plexiglass plate, bonded to a 3.2-cm-thick block of styrene insulation. The edges of the wall which bounded the vent were beveled back at 60° in order to minimize the resistance experienced by the fluid flowing from the ambient to the vent

opening in the channel wall. The bevel was continued back into the insulation and then terminated to provide a plenum chamber for the incoming fluid. Several sets of upper and lower walls with different heights were employed during the experiments to obtain the desired vent openings and axial positions.

Precisely machined spacers were employed in setting the interwall spacing S. A dial-equipped caliper with accuracy of 0.0025 cm was utilized in verifying both the interwall spacing and the vent opening. Plexiglass side walls were attached to the two principal walls completing the channel geometry. Plexiglass was chosen as the side wall material to allow visual observation of the flow patterns inside the channel during the flow visualization experiments.

The test environment

The experiments were conducted in a fluid environment free of extraneous buoyancy-induced motions. This was accomplished by a system of two chambers both of which were filled with distilled water. The chambers were created by the use of two Plexiglass tanks, one placed within the other. The respective dimensions of the inner and outer tanks were $73.1 \times 43.2 \times 45.3$ cm and $101.6 \times 66.0 \times 48.3$ cm (length × width × height). Heat and water losses due to evaporation were eliminated by covering the tops of the two tanks.

The heat transfer and flow visualization experiments were performed in the inner chamber, while the outer chamber provided thermal control. This was achieved by installing a temperature controller and water circulating unit in the space between the inner and outer tanks. This unit provided an agitated bath around the inner tank at a pre-selected temperature. The temperature level was maintained to achieve a nominal Prandtl number of 5 during the experiments.

The test section described earlier was mounted on a Plexiglass supporting frame (not shown in Fig. 1) and placed in the inner tank. Special care was taken in the design of the supporting frame to avoid obstruction of the flow in the vicinity of the channel openings. A 12.7-cm vertical clearance existed between the inlet of the channel and the floor of the inner tank and between the exit of the channel and the free surface of the water.

Three pre-calibrated chromel–constantan thermocouples (0.0254-cm diam.) were vertically deployed in the inner tank to sense possible undesirable temperature stratifications in the water.

As will be seen shortly in the description of the experimental procedure, equality between the water temperature in the inner and outer chambers was a necessary condition for the initiation of a data run. This temperature equality was verified by a 0.1°C ASTM-certified thermometer installed in each chamber.

Temperature probe

To facilitate measurement of temperature profiles in the interwall space, a special thermocouple probe was designed and fabricated. As shown pictorially in Fig. 2, the probe consisted of a two-pronged fork between whose tines the thermocouple was stretched. The thermocouple was made from bare 0.0076-cm-diam. chromel and constantan wire that had been pre-calibrated. The junction, situated midway between the tines, was formed by a butt-welding operation such that the chromel lead wire extended between the junction and one of the tines, and the constantan lead wire extended between the junction and the other tine.

As seen in the figure, the tines of the fork were positioned adjacent to the respective side walls of the channel in order to avoid flow disturbances in the channel proper. For the same reason, the horizontal member of the fork was situated outside the channel. The stem atop the fork was connected to a traversing mechanism which was capable of positioning the junction to 0.001 in.

Experimental procedure for heat transfer runs

The preparation for a data run was initiated by setting the desired interwall spacing, vent opening size, and vent axial position according to the procedures described earlier. The test section was then mounted on the supporting frame, placed in the inner chamber, and leveled.

Next, the equality of the temperatures of the water in the outer and inner chambers was verified by reading the thermometers. This equality in temperature guaranteed that the inner tank was free of extraneous, buoyancy-induced motions. Then, the power settings of the three heaters were dialed in. Previous experience furnished the relationship among the power settings that would yield uniform temperature at the heated wall. Power to the heaters was then switched off but the settings maintained. The water in the inner tank was manually stirred to eliminate temperature stratification. The attainment of the non-stratified condition was verified by the readings of the three thermocouples deployed in the inner chamber. An hour waiting period was allowed for the motions generated by the stirring operation to die away.

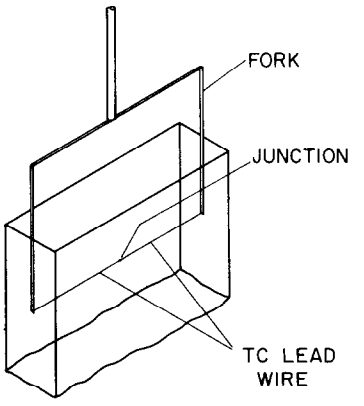

FIG. 2. Thermocouple probe in place in the channel.

After this waiting period, power was again delivered to the heaters, and the attainment of steady-state conditions was verified by monitoring selected plate thermocouples. At steady state, the plate and water temperatures, voltages, and currents were recorded, and a new setting of the voltages for the next data run was dialed in, after which the power was switched off. The water in the tank was stirred, and after another hour waiting period, a new data run could be performed.

In order to provide baseline information for comparison with the results obtained for the ventilated channel, heat transfer runs were also performed with the vent opening closed. For this purpose, the vent opening was blocked with thin polyester tape (0.002-cm thick) so as to totally suppress fluid flow through the opening without, however, altering the thermal boundary conditions at the unheated wall which prevailed during the experiments for the ventilated channels. As will be shown in the presentation of the results, baseline information was obtained for each investigated channel spacing, heated wall to ambient temperature difference, vent opening, and axial position.

Experimental procedure for temperature profile runs

To prepare for the measurement of the fluid temperature profiles, the probe described earlier was introduced into the channel and the axial position set with the aid of a cathetometer. Then, using electrical contact between the thermocouple junction and the copper wall, a reference position for the junction was established. The probe was then traversed so that the center of the junction was 0.0254 cm from the surface of the copper wall, and this position served as the first station for the traverse that was subsequently performed.

At this point of time, the procedure that was already described for the heat transfer data runs was executed, and when steady state was achieved, the traverse was initiated. All told, 43 temperature measurements were made in the interwall space at positions which will be evident from the data to be presented later. About 15 min were required to complete a traverse.

Temperature profiles were determined both for the ventilated channel and for the corresponding non-ventilated channel.

Flow visualization experiments

Flow visualization experiments were conducted with the objective of revealing the flow patterns in the vicinity of the vent. This was accomplished by employing the thymol blue method [4]. This is an electrochemical technique where the fluid undergoes a change in color in response to a change in pH due to an imposed DC voltage. The tracer fluid generated is neutrally buoyant and faithfully follows the flow. Three substances are added to the water in order to enable the generation of the tracer fluid: a pH indicator (thymol blue), an acid (hydrochloric acid), and a base (sodium hydroxide). Due to the addition of these substances, the flow visualization runs were performed separately from the heat transfer runs.

To implement the method, two copper electrodes are placed in the solution and, if a small DC voltage (less than 6 V) is imposed, a change in the pH of the solution in the neighborhood of the negative electrode produces the tracer fluid. By placing the negative electrode in a suitable location, the flow patterns of interest can be observed.

In the present experiments, the negative electrode consisted of three 14-gauge copper wires shown in Fig. 1 and labeled *tracer fluid sources*. Each wire extended across the span of the test section. A copper-foil electrode (0.00254-cm thick) bonded to the beveled surface of the lower edge of the vent opening was used to provide additional tracer fluid. A typical photograph of the flow field revealed by these electrodes will be presented later.

The preparation for a flow visualization run included the same procedures described for the heat transfer runs, i.e. setting of the interwall spacing and vent geometry, inter-tank temperature equilibration, stirring, one-hour waiting period, and observation of the attainment of the steady-state condition. At this point, voltage from an adjustable DC power supply was applied to the electrochemical circuit.

Photographs of the flow field were obtained with a 100-mm Pentax macro lens utilizing black and white film (Kodak Tri-X, 400 ASA).

Data reduction

The experimentally determined heat transfer results will be presented in this paper in terms of the Nusselt and Rayleigh numbers. These dimensionless quantities were calculated from the experimental data, following the procedure which will now be outlined.

The Nusselt number was evaluated from

$$Nu_s = hS/k, \quad h = Q/A(T_w - T_\infty) \tag{1}$$

where Q is the rate of convective heat transfer to the fluid, and A is the area of the heated plate.

A one-dimensional heat conduction calculation demonstrated that heat losses through the backing insulation of the heated plate were negligible. Therefore, Q was taken as the electrical power input to the plate without any corrections.

The wall temperature T_w was calculated by averaging the readings of the eight plate thermocouples. Similarly, the ambient temperature T_∞ was obtained by averaging the readings of the three thermocouples deployed in the inner chamber.

The Rayleigh number based on the interwall spacing was calculated from

$$Ra_s = [g\beta(T_w - T_\infty)S^3/\nu^2]\, Pr \tag{2}$$

where all the thermophysical properties were evaluated at the film temperature $\frac{1}{2}(T_w + T_\infty)$.

NUMERICAL ANALYSIS

A numerical study of the heat transfer and fluid flow characteristics of the one-sided heated ventilated channel was conducted to supplement the experimental work. A schematic view of the calculation domain utilized is presented in Fig. 3, where the coordinates and the relevant geometric parameters are defined. The analysis was based on the two-dimensional conservation equations incorporating the standard boundary-layer approximations and the Boussinesq model for the density variation.

For the coordinate system shown in Fig. 3, the dimensionless form of the governing equations can be written as [5]

$$\partial U/\partial X + \partial V/\partial Y = 0 \tag{3}$$

$$U(\partial U/\partial X) + V(\partial U/\partial Y) = -\mathrm{d}P/\mathrm{d}X + \theta + \partial^2 U/\partial Y^2 \tag{4}$$

$$U(\partial\theta/\partial X) + V(\partial\theta/\partial Y) = (1/Pr)(\partial^2\theta/\partial Y^2) \tag{5}$$

where

$$X = (x/S)/Gr_s, \quad Y = y/S \tag{6}$$

$$U = (uS/\nu)Gr_s, \quad V = vS/\nu \tag{7}$$

$$P = p'(x)(S^2/\rho\nu^2)/Gr_s^2, \quad \theta = (T - T_\infty)/(T_w - T_\infty). \tag{8}$$

In the dimensionless pressure, equation (8), $p'(x)$ is equal to $p(x) - p_\infty(x)$, which is the imbalance between the pressures within the channel and in the ambient at a given axial position x.

The boundary conditions at the heated wall ($Y = 0$) can be written as

$$U = V = 0, \quad \theta = 1. \tag{9}$$

At the entrance of the channel ($X = 0$), the velocity was assumed to be uniform and the temperature of the incoming fluid was taken as equal to the ambient temperature, so that

$$U = U_o, \quad V = 0, \quad \theta = 0. \tag{10}$$

The pressure at the entrance of the channel was obtained from Bernoulli's equation which, in dimensionless form, becomes

$$P = -\tfrac{1}{2}U_o^2. \tag{11}$$

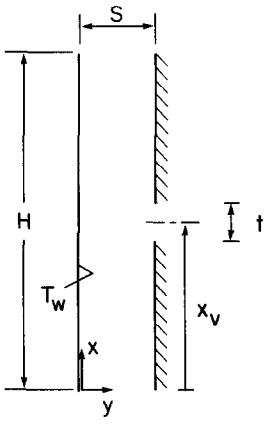

FIG. 3. Schematic view of the calculation domain.

At the exit plane ($X = H/S\,Gr_s$), the pressure within the channel was assumed to be identical to the ambient pressure, so that

$$P = 0. \tag{12}$$

Attention is now focused on the boundary conditions at the vent opening. The opening is centered at the axial coordinate x_v, and its upstream and downstream edges are located at

$$x_1 = x_v - \tfrac{1}{2}t, \quad x_2 = x_v + \tfrac{1}{2}t \tag{13}$$

The velocity boundary condition at the vent opening was determined by assuming that fluid entered the channel horizontally, driven by the pressure difference $p'(x) = p(x) - p_\infty(x)$. Consistent with the practice used at the channel inlet, Bernoulli's equation was also employed in the determination of the transverse velocity at the vent. This approach was adopted because the Bernoulli description of the pressure at the channel inlet $X = 0$ is well supported by the excellent agreement of numerically and experimentally determined average Nusselt numbers for unvented, one-sided heated channels [6].

At any X in the vent opening, Bernoulli's equation yields, in dimensionless terms,

$$V(X) = (-2P\,Gr_s^2)^{1/2} \tag{14}$$

and by assumption

$$U = 0 \tag{15}$$

for $Y = 1$ and $X_1 < X < X_2$, where

$$X_1 = X_v - \frac{1}{2}\frac{t/S}{Gr_s} \tag{16}$$

$$X_2 = X_v + \frac{1}{2}\frac{t/S}{Gr_s}. \tag{17}$$

Again, as at the inlet of the channel, the temperature of the fluid entering the vent was taken as the ambient temperature, so that the thermal boundary condition at the vent-opening region ($Y = 1$ and $X_1 < X < X_2$) becomes

$$\theta = 0. \tag{18}$$

For the sections of the unheated wall other than the vent, zero velocity and heat flux conditions were imposed

$$U = V = 0 \quad \text{and} \quad \partial\theta/\partial Y = 0. \tag{19}$$

Solution procedure

An examination of the conservation equations and boundary conditions presented in the foregoing reveals that the problem depends on five prescribable parameters: the Grashof number Gr_s, the Prandtl number Pr, and the dimension ratios S/H, x_v/H, and t/S. In addition, it appears that the dimensionless entrance-section velocity U_o is also a prescribable parameter. However, it will soon be demonstrated that U_o is not independently prescribable.

The natural convection problem described by equations (3)–(5) and (9)–(19) was solved by the Patankar–Spalding finite-difference method. This scheme is a forward-marching procedure which requires that temperature and velocity be specified at $X = 0$. For a fixed dimensionless height of the channel $H/S\ Gr_s$, the magnitude of the entrance velocity U_o had to be adjusted so that the condition $P = 0$ at the exit of the channel was satisfied. This was achieved iteratively by utilizing a Newton–Raphson procedure. Thus, U_o was chosen to satisfy the pressure boundary condition and, therefore, it is not an independently prescribable parameter.

The desired numerical accuracy was obtained by employing 600×52 grid points (streamwise $\times$ cross-stream directions).

From the numerical solutions, the local Nusselt number at any axial location on the heated wall was calculated from

$$Nu_{loc} = qS/(T_w - T_\infty)k = -(\partial\theta/\partial Y)_{Y=0} \quad (20)$$

where

$$q = -k(\partial T/\partial y)_{y=0}. \quad (21)$$

The total heat transfer from the heated wall was calculated from

$$Q = \int_0^H -k(\partial T/\partial y)_{y=0}\,dx \quad (22)$$

from which the average Nusselt number was evaluated as

$$Nu_s = [Q/H(T_w - T_\infty)](S/k) = (S/H)\,Gr_s \int_0^{H/S\,Gr_s} [-(\partial\theta/\partial Y)_{Y=0}\,dX]. \quad (23)$$

The ratio of the mass flow rate entering the channel through the vent opening to the mass flow rate entering the channel via the main opening was obtained from

$$\dot{m}_{vent}/\dot{m}_o = \left[\int_{x_1}^{x_2} \rho v(x)\,dx\right] \Big/ \rho u_0 S = (1/U_o)\int_{X_1}^{X_2} V(X)\,dX. \quad (24)$$

RESULTS AND DISCUSSION

As mentioned in the Introduction, the objective of the present work is to investigate how the heat transfer and fluid flow in a vertical, one-sided-heated channel is affected by fluid entering the channel through a vent in the unheated wall. The research program conducted to achieve this goal encompassed the experimental determination of average Nusselt numbers and of temperature profiles across the channel, flow visualization, and numerical solutions.

Average Nusselt number results

Average Nusselt numbers for the heated wall were determined experimentally for three values of the dimensionless interwall spacing S/H. For each spacing, two vent opening sizes t/S were studied with the vent at three different axial positions X_v. For a particular geometrical configuration defined by S/H, t/S, and X_v, the Rayleigh number Ra_s was varied by an order of magnitude by varying the temperature difference between the heated wall and the fluid environment. For the presentation of the results, the $(S/H)Ra_s$ group was used as the abscissa variable because it is commonly employed for unvented channels. For comparison purposes, experiments were also performed with the vent opening closed, as described in the experimental procedure section.

Average Nusselt number results are presented as a function of the channel Rayleigh number $(S/H)Ra_s$ in Figs. 4–6, respectively, for dimensionless interwall spacings $S/H = 2.19 \times 10^{-2}$, 3.24×10^{-2}, and 6.56×10^{-2}. Each figure presents data for two different dimensionless vent opening sizes t/S, denoted by open and black symbols, which are defined in the legend at the top of the figures. For each opening size, results for three vent axial positions are displayed: lower, mid, and upper. The actual values of the vent axial positions corresponding to these designations can be found in Table 1. To avoid overlapping of the data, individual graphs were employed for each case. Each graph includes two sets of data. The results for the baseline case (vent opening closed) are represented by circles while squares denote the data obtained for the vented channels. Lines were fitted through the baseline data to provide continuity.

An overall inspection of Figs. 4–6 reveals that the average Nusselt number for the channel is insensitive to either the vent opening size or the axial location of the vent, for the range of parameters investigated. Indeed, the maximum deviation of the data for the vented channel from the baseline data is under 2%, which is of the same magnitude as the expected scatter of the data. The experimentally determined insensitivity of the average Nusselt number to the presence of the vent was corroborated by the numerical solutions.

The aforementioned insensitivity can be rationalized with the aid of the numerical results. The numerically obtained rates of mass flow entering the channel through the principal (bottom) opening and the vent

Table 1. Axial coordinates at the center of the vent opening

		x_v/H		
S/H	t/S	Lower	Mid	Upper
2.19×10^{-2}	2.0	0.127	0.5	0.873
	4.0	0.149	0.5	0.851
3.24×10^{-2}	1.0	0.121	0.5	0.879
	2.0	0.137	0.5	0.863
6.56×10^{-2}	0.5	0.121	0.5	0.879
	1.0	0.138	0.5	0.862

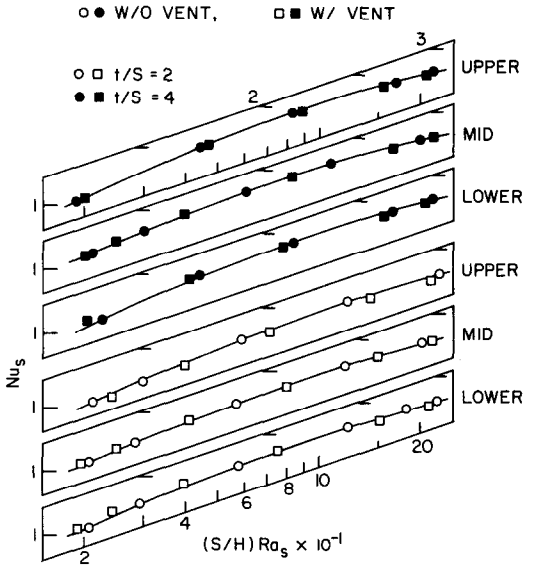

FIG. 4. Average Nusselt numbers for vented and unvented channels, $S/H = 2.19 \times 10^{-2}$.

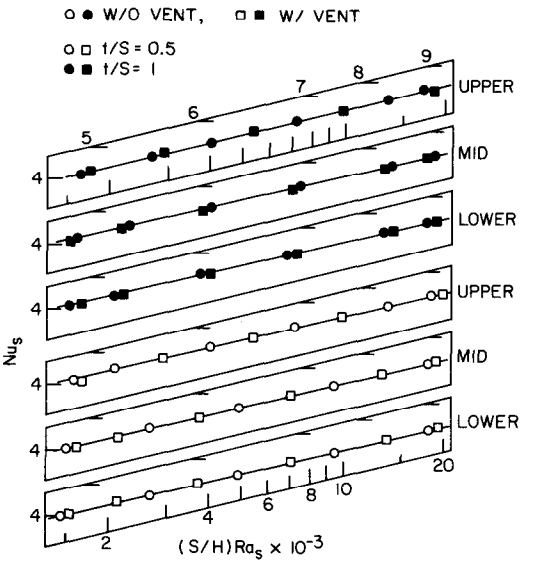

FIG. 6. Average Nusselt numbers for vented and unvented channels, $S/H = 6.56 \times 10^{-2}$.

opening are presented in Fig. 7 as a function of the vent opening size and axial position, for the typical values of $(S/H)Ra_s$ and (S/H) indicated there. In this figure, the left ordinate represents the ratio between the mass flow rate entering the channel via the vent opening $\dot{m}_{vent}$ and the mass flow rate entering the channel through its principal opening $\dot{m}_o$. The right ordinate is the ratio of the total mass flow $\dot{m}_{tot}$ drawn into the channel through the two openings to the mass flow rate $\dot{m}_{no/vent}$ drawn through the unvented channel. The two ordinates employ the same scale and are designated according to the arrows shown in the figure.

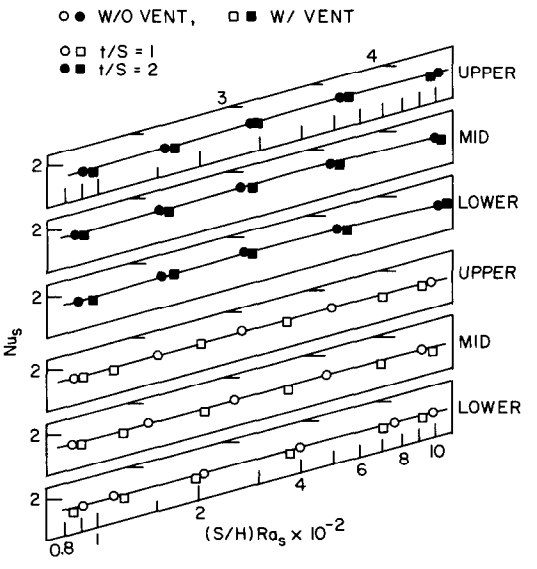

FIG. 5. Average Nusselt numbers for vented and unvented channels, $S/H = 3.24 \times 10^{-2}$.

It can be noted from the figure that while there is a sharp increase in the ratio $\dot{m}_{vent}/\dot{m}_o$ as the vent opening size increases, the total mass flow rate drawn through the channel is only slightly affected by the presence of the vent opening, i.e. the ratio $\dot{m}_{tot}/\dot{m}_{no/vent}$ remains close to unity. In particular, when the vent opening is at the lower position, no change is observed in the total mass flow rate due to the presence of the vent, i.e. $\dot{m}_{tot}/\dot{m}_{no/vent} \cong 1$. For the other positions of the opening, the increase in the total flow due to the vent is about 10%.

From a careful examination of the figure, it may be concluded that the presence of the vent opening is seen to always decrease the mass flow rate through the principal opening of the channel. As a result, it is expected that the heat transfer at axial stations below

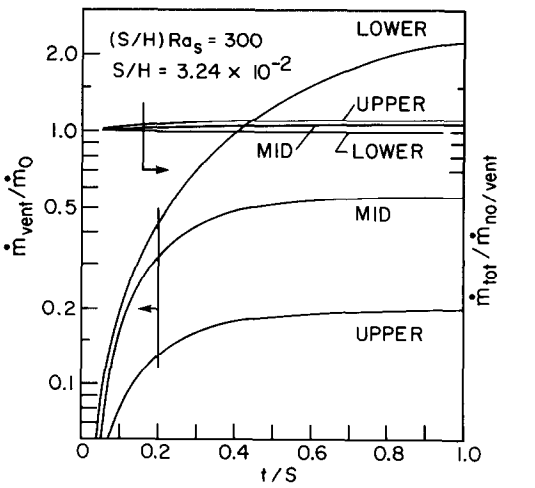

FIG. 7. Typical results for the flow rates entering the channel.

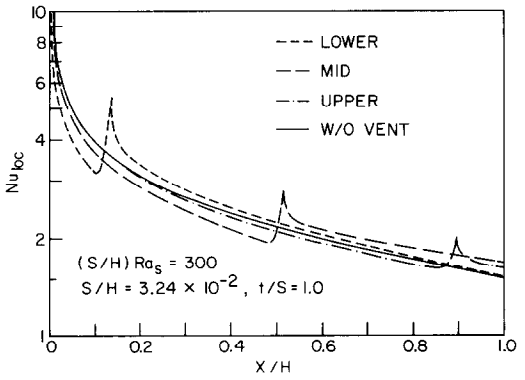

FIG. 8. Typical local Nusselt number distributions on the heated wall.

the vent should be less than that in the corresponding unvented channel. However, since the vent opening delivers a stream of relatively cool fluid to the channel, it is expected that the heat transfer at and above the vent opening will be enhanced. These vent-related opposing effects are, seemingly, mutually canceling as witnessed by the insensitivity of the Nusselt number results of Figs. 4—6 to the presence of the vent.

Local Nusselt number results

Numerically obtained local Nusselt numbers are presented in Fig. 8 as a function of the dimensionless axial position x/H for typical values of $(S/H)Ra_s$, S/H, and t/S. The solid line in the figure represents the distribution of the local Nusselt number for the unvented channel (i.e. the baseline case), while the other lines represent the results for the three axial positions of the vent opening, as indicated by the legend.

The most striking feature of the figure is the sharp peak exhibited by the local Nusselt number in response to the presence of the vent opening. The height of the peak is less pronounced at vent locations higher in the channel. This decrease in the peak occurs because less mass flow is drawn into the channel through a higher-positioned vent than a lower-positioned vent. Further examination of the figure shows that upstream of the vent position the local Nusselt number for the channel is lower than that for the unvented channel. Downstream of the vent, the opposite relationship applies.

Cross-channel temperature profiles

The effect of the presence of the vent opening on the temperature field within the channel was revealed by examining cross-channel temperature profiles at different axial positions. To this end, Fig. 9 was prepared to convey the numerically determined temperature profiles at four axial locations for typical values of $(S/H)Ra_s$, S/H, and t/S with the vent opening situated at the mid-height position. The dimensionless temperature $(T-T_\infty)/(T_w-T_\infty)$ is plotted as a function of the dimensionless cross-stream coordinate y/S, which varies from 0 (heated wall) to 1 (unheated wall). The profiles presented correspond to four different axial positions labeled I, II, III, and IV, which are defined in the schematic view of the channel shown in the inset of Fig. 9. For each axial position, temperature profiles for the vented channel (solid lines) and for the unvented channel (dashed lines) are compared. To avoid overlapping of the profiles, the ordinate origins were displaced.

At the axial station just below the vent opening (position I), the temperature profile for the vented case lies above the profile for the unvented case, reflecting the lesser mass flow rate passing through this portion of the channel when the vent opening is present. At the vent, the cooler fluid entering the channel lowers the temperature of the channel flow. At the centerline of

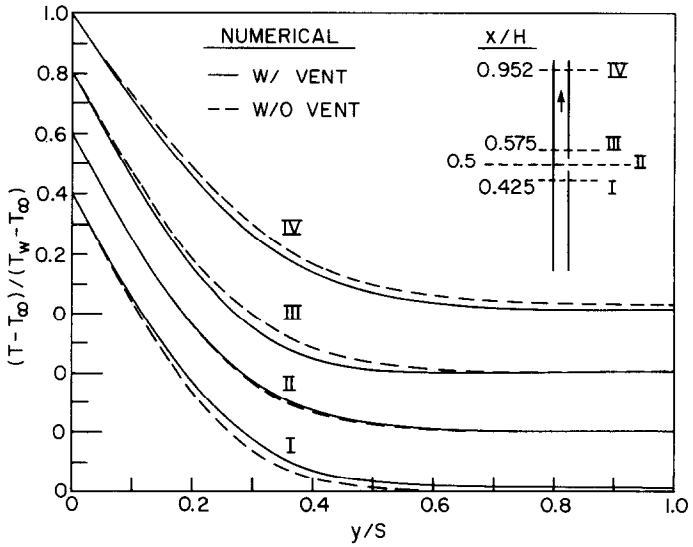

FIG. 9. Numerically determined cross-channel temperature distributions for vented and unvented channels for $S/H = 6.56 \times 10^{-2}$, $(S/H)Ra_s = 1.7 \times 10^3$, $t/S = 1.0$, $x_v/H = 0.5$.

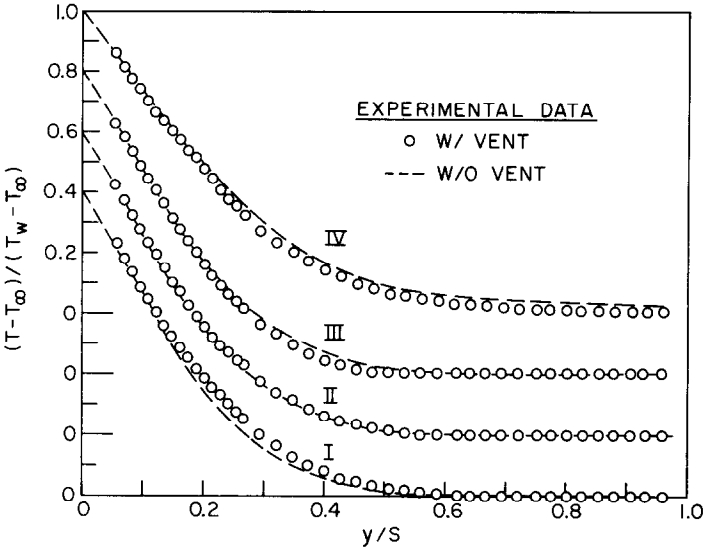

FIG. 10. Experimentally determined cross-channel temperature distributions for vented and unvented channels for $S/H = 6.56 \times 10^{-2}$, $(S/H)Ra_s = 1.7 \times 10^3$, $t/S = 1.0$, $x_v/H = 0.5$.

the vent opening (position II), the two profiles for the unvented and vented cases are nearly indistinguishable. Above the vent (positions III and IV), the effect of the cooler fluid admitted through the vent opening persists, giving rise to temperature profiles which lie below those for the unvented channel, as can be verified by comparing the temperature profiles for the vented and unvented cases at positions III and IV.

Temperature profiles were also obtained experimentally for the very same set of parameters that characterized the numerical results of Fig. 9. The experimentally determined temperature profiles are presented in Fig. 10 in the same format as was used in Fig. 9. The experimental data for the vented case are represented by circles. The dashed lines represent the temperature profiles for the unvented channel obtained by fitting the experimental data. The actual data points were not plotted to avoid severe overlap.

An examination of Fig. 10 leads to the same conclusions as were drawn from the numerically determined results of Fig. 9 regarding the evolution of the temperature along the channel. Indeed, the details of the relationship between the unvented and vented cases displayed in Fig. 9 are perfectly reproduced in Fig. 10.

A direct comparison of the numerically and experimentally determined temperature profiles is provided in Fig. 11. Two axial stations in the channel were chosen for comparison (locations II and IV). At each station, numerically and experimentally determined profiles were plotted for both the vented and the unvented channels. The ordinate origins were displaced to avoid overlapping and should be used in accordance with the arrows shown in the figure.

As the figure indicates, the agreement between the numerical predictions and the measured data can be considered excellent for both the vented and the unvented channels. The same level of agreement was encountered for other axial locations (not presented due to space limitations).

Flow visualization results

The flow visualization experiments had the objective of revealing the flow patterns in the vicinity of the vent opening. Figure 12 is a photograph illustrating the flow field obtained by employing the techniques and procedures described earlier in this paper. The photograph shows a side view of the vent opening and the adjacent portions of the channel and of the fluid region outside the channel. The photograph corresponds to the mid-height position of the vent and to $S/H = 6.56 \times 10^{-2}$, $t/S = 1.0$, and $(S/H)Ra_s = 2 \times 10^4$. In the photograph, the white vertical strip, interrupted by the vent opening, is the unheated Plexiglass wall. The black vertical strip at the left is the heated copper wall.

The dark, nearly horizontal streamers to the right of the vent opening shown in the photograph were produced by the tracer fluid generated at three horizontal electrodes (not shown in Fig. 12 but shown schematically in Fig. 1). These streamers are seen to converge as they pass into the vent opening. After entering into the channel, part of the fluid flows upward and part flows downward along the unheated wall. To better resolve the downflow, a copper foil electrode situated on the lower beveled edge of the vent was used to provide additional tracer fluid. The downward-moving fluid reaches a maximum penetration and then turns and flows upward, forming a V-shaped recirculation region. Within this recirculation zone, fluid moves downward along the unheated wall and upward along the left leg of the V-shaped region.

A very similar recirculation pattern was described in ref. [3] for the upper region of a one-sided-heated,

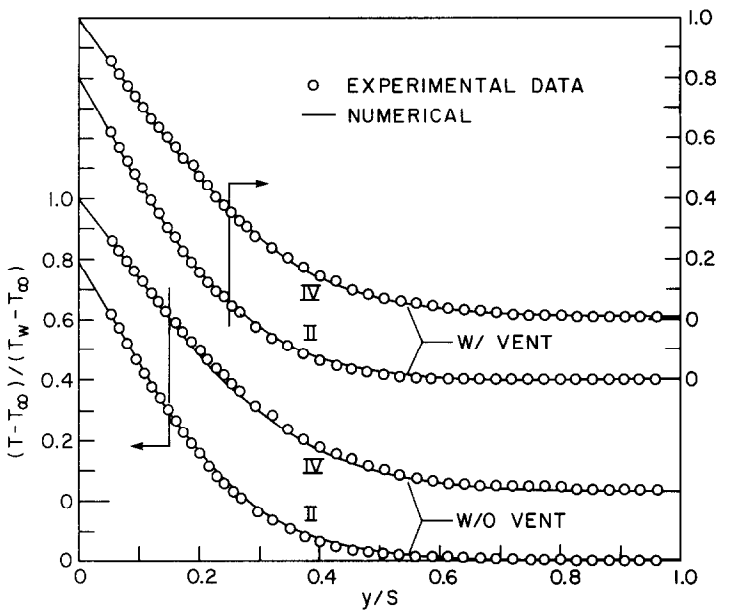

FIG. 11. Comparison of experimentally and numerically determined cross-channel temperature profiles for $S/H = 6.56 \times 10^{-2}$, $(S/H)Ra_s = 1.7 \times 10^3$, $t/S = 1.0$, $x_v/H = 0.5$.

unvented, vertical channel. The arguments presented there for the existence of the pocket of recirculating flow can be extended to the present situation.

It is relevant to note that the partitioning of the vent flow in upflow and downflow portions did not occur for all operating conditions. In particular, at small surface-to-ambient temperature differences, the entire vent flow moved upward in the channel. It is also noteworthy that for all the investigated operating conditions, the flow through the vent was always from the ambient into the channel and not vice versa.

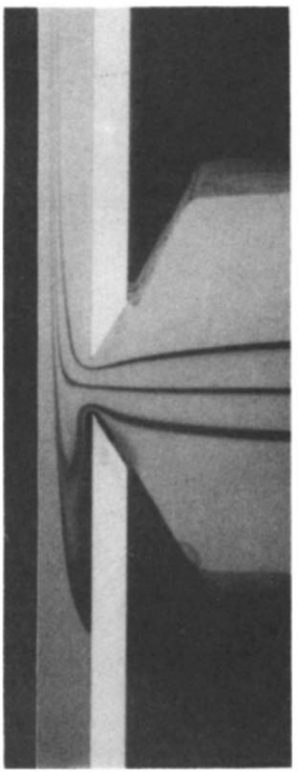

FIG. 12. Flow visualization pattern in the vicinity of the vent opening for $S/H = 6.56 \times 10^{-2}$, $(S/H)Ra_s = 2 \times 10^4$, $t/S = 1.0$, $x_v/H = 0.5$.

CONCLUDING REMARKS

The present investigation examined the response of the natural convection heat transfer and fluid flow characteristics of one-sided-heated channels to fluid entering the channel through a vent in the unheated wall. The work encompassed both experiments and complementary numerical solutions.

Average Nusselt numbers were experimentally determined for parametric variations of the dimensionless interwall spacing, vent opening size, and vent axial location. For each configuration defined by these geometrical parameters, the wall-to-ambient temperature difference was varied by an order of magnitude while the Prandtl number of the working fluid (water) was maintained at a nominal value of 5. In order to provide baseline data, experiments were also performed for the corresponding unvented channel. Information on the temperature field within the channel was obtained by measuring cross-channel temperature profiles at different axial positions for both vented and unvented channels. Flow visualization experiments were conducted to reveal the patterns of fluid flow in the vicinity of the vent opening.

Finite-difference-based numerical solutions were obtained for the parabolic form of the conservation equations. These solutions yielded both local and

average Nusselt numbers, cross-channel temperature distributions, and rates of fluid flow passing into the channel through both the principal opening (at the bottom of the channel) and through the vent.

The experimental results demonstrated that, for the range of parameters investigated, the average Nusselt numbers for the channel were insensitive to both the vent opening size and the axial location of the vent. This finding was corroborated by the numerical solutions. The solutions indicated that although the presence of the vent opening causes a decrease in the mass flow rate entering the principal opening of the channel, the total mass flow drawn into the channel is only slightly affected.

The numerically determined local Nusselt number distributions along the heated wall exhibited sharp peaks in response to the relatively cool fluid entering the channel via the vent opening. However, upstream of the vent position, the local Nusselt number was shown to be lower than that for the unvented channel due to the lesser mass flow rate passing through that portion of the channel. Numerically and experimentally determined cross-channel temperature profiles displayed excellent agreement, revealing the effects of the presence of the vent opening on the temperature field.

Flow visualization experiments demonstrated that, for certain operating conditions, part of the fluid entering the vent flows upward and part flows downward along the unheated wall. Upon reaching a maximum depth of penetration, the downward moving fluid turns and flows upward forming a V-shaped recirculation zone.

Acknowledgement—Support accorded to L. F. A. Azevedo by Conselho Nacional de Desenvolvimento Científico e Tecnológico (CNPq) of Brazil is gratefully acknowledged.

REFERENCES

1. W. Aung, L. S. Fletcher and V. Sernas, Developing laminar free convection between vertical flat plates with asymmetric heating, *Int. J. Heat Mass Transfer* **15**, 2293–2308 (1972).
2. O. Miyatake and T. Fujii, Free convective heat transfer between vertical plates—one plate is isothermally heated and the other is thermally insulated, *Heat Transfer–Jap. Res.* **1**(3), 30–38 (1972).
3. E. M. Sparrow, G. M. Chrysler and L. F. Azevedo, Observed flow reversals and measured-predicted Nusselt numbers for natural convection in a one-sided heated vertical channel, *J. Heat Transfer* **106**, 325–332 (1984).
4. D. J. Baker, A technique for the precise measurement of small fluid velocities, *J. Fluid Mech.* **26**, 573–575 (1966).
5. J. R. Bodoia and J. F. Osterle, The development of free convection between heated vertical plates, *J. Heat Transfer* **84**, 40–44 (1962).
6. E. M. Sparrow and L. F. A. Azevedo, Vertical-channel natural convection spanning between the fully developed limit and the single-plate boundary layer limit, *Int. J. Heat Mass Transfer* **28**, 1847–1857 (1985).

CONVECTION NATURELLE DANS UN CANAL VERTICAL VENTILE A TRAVERS UNE OUVERTURE DANS LA PAROI DU CANAL

Résumé—On étudie expérimentalement et numériquement la convection naturelle dans un canal vertical chauffé sur un coté avec une ouverture sur la paroi non chauffée. Les expériences sont faites avec de l'eau ($Pr \simeq 5$) pour des variations paramétriques de l'espacement, de la dimension de l'évent, de la position axiale de celui-ci et de la différence de température entre paroi et ambiance (nombre de Rayleigh). Pour comparaison, des données sont aussi obtenues pour des canaux normaux. Les résultats thermiques sont complétés par des mesures de distribution de température et par une visualisation de l'écoulement à l'aide de la technique électrochimique au bleu de thymol. Les solutions numériques donnent une information à la fois sur les nombres de Nusselt locaux et moyens, sur les profils de température dans une section droite et sur les débits de fluide à travers la base du canal et à travers l'évent. Les expériences et les solutions numériques montrent que les nombres de Nusselt moyens pour le canal sont insensibles à la dimension de l'évent et à sa position axiale pour le domaine des conditions opératoires considéré. Les solutions numériques montrent que bien que le débit masse entrant par la base du canal décroisse du fait de la présence de l'event, le débit total dans le canal est peu affecte. Un excellent accord est constaté entre les profils de température expérimentaux et calculés. Pour certaines conditions opératoires, les expériences de visualisation révèlent l'existence d'une zone de recirculation à l'intérieur du canal, adjacente au bord inférieur de l'évent.

NATÜRLICHE KONVEKTION IN EINEM VERTIKALEN KANAL, DER DURCH EINE ÖFFNUNG IN DER KANALWAND MIT DER UMGEBUNG VERBUNDEN IST

Zusammenfassung—Die natürliche Konvektion in einem einseitig beheizten vertikalen Kanal, der durch eine Öffnung in der unbeheizten Wand mit der Umgebung verbunden ist, wurde sowohl experimentell als auch numerisch untersucht. Die Experimente wurden in Wasser durchgeführt ($Pr \cong 5$), wobei der Wandabstand, die Größe der Öffnung, die axiale Lage der Öffnung und die Temperaturdifferenz zwischen Wand und Umgebung (Rayleigh-Zahl) variiert wurden. Für Vergleichszwecke wurden die Basisdaten auch für ungeöffnete Kanäle ermittelt. Die Ergebnisse bezüglich der Wärmeübertragung wurden durch Messungen der Temperaturverteilung im Kanalquerschnitt und durch Sichtbarmachung der Strömung mit dem elektrochemischen Thymolblauverfahren ergänzt. Die numerischen Lösungen ergaben Informationen über die örtlichen und mittleren Nusselt-Zahlen, die Temperaturprofile im Kanalquerschnitt und über den Stoffaustausch durch die Öffnung am Kanalboden und durch die Öffnung in der Wand. Die Experimente und die numerischen Lösungen zeigten, daß im untersuchten Parameterbereich die mittleren Nusselt-Zahlen für den Kanal hinsichtlich der Größe und der axialen Lage der Öffnungen unempfindlich sind. Die numerischen Lösungen zeigten, daß der Gesamtmassenstrom, der in den Kanal eindringt, nur sehr wenig beeinflußt wird, obwohl der Massenstrom durch die Öffnung am Boden wegen der Öffnung in der Wand abnimmt. Die örtlichen Nusselt-Zahlen zeigten aufgrund der Öffnung ausgeprägte Spitzen. Es konnte eine hervorragende Übereinstimmung zwischen experimentell und numerisch ermittelten Temperaturprofilen quer zum Kanal erzielt werden. Für ganz bestimmte Betriebsbedingungen offenbarten die Experimente zur Sichtbarmachung der Strömung die Existenz einer Rückströmzone im Kanal, und zwar gegenüber der unteren Kante der Wandöffnung.

ЕСТЕСТВЕННАЯ КОНВЕКЦИЯ В ВЕРТИКАЛЬНОМ КАНАЛЕ, СООБЩАЮЩЕМСЯ С ОКРУЖАЮЩЕЙ СРЕДОЙ ЧЕРЕЗ ОТВЕРСТИЕ В СТЕНКЕ

Аннотация—Экспериментально и численно исследовалась естественная конвекция в вертикальном канале, одна из стенок которого нагревалась, а в другой имелось вентиляционное отверстие. Эксперименты выполнялись для воды ($Pr \cong 5$) при параметрических изменениях расстояния между стенками, размера вентиляционного отверстия, его расположения относительно оси канала и разности температур стенки и окружающей среды (число Рэлея). Для сравнения были также получены основные характеристики для каналов, не имеющих отверстий в стенках. Кроме данных по теплопереносу измерены распределения температуры в поперечных сечениях каналов и с помощью электрохимической методики тимоловой сини визуализированы потоки. Численные расчеты позволили получить информацию о локальных и средних числах Нуссельта, температурных профилях в поперечных сечениях каналов и скоростях движения жидкости через отверстие в нижней части канала и вентиляционное отверстие. Экспериментальные и численные результаты показали, что в исследованном диапазоне эксплуатационных условий средние числа Нуссельта для канала с вентиляционным отверстием не зависят от размера отверстия и его положения относительно оси канала. Из численных расчетов следует, что хотя расход массы через отверстие в нижней части канала уменьшается при наличии вентиляционного отверстия, суммарный расход массы, втекающей в канал, изменяется при этом незначительно. При наличии вентиляционного отверстия в распределениях локальных чисел Нуссельта существуют резкие максимумы. Между экспериментально и численно определенными температурными профилями в поперечных сечениях канала имеется очень хорошее согласие. При некоторых условиях с помощью визуализации была обнаружена зона рециркуляции, примыкающая к нижнему краю вентиляционного отверстия.